7. Fe/Tb multilayers with variant number of bilayers

In our previous studies on MLs with diamagnetic blocking layers (Chap. 6) it has been shown that the PMA induced by the Fe/Tb interfaces is suppressed by the intercalated diamagnetic Y or Ag layers. In order to study correlations between the number of the interfaces and the PMA, samples with 1 to 20 Fe/Tb interfaces were prepared and investigated by means of MOKE and CEMS. As outlined in Chap. 4 thicknesses $t_{Fe} = 3.5$ nm and $t_{Tb} = 1.4$ nm are used throughout. According to the phase diagram, Fig. 5.8, c-Fe and a-Tb are encountered in these samples. In this Chapter the influence of the number n of Fe/Tb bilayers on the PMA and on the magnetization reversal studied by in situ MOKE will be presented. In particular changes in the shape of the Kerr hysteresis cycles were studied as a function of n. Variations of both, rectangularity and coercivity, indicate the influence of different Fe modifications and are discussed in terms of growth-induced structural changes. This is also evidenced in the wavelength dependence of the saturated Kerr ellipticity ε_K^s. An analysis of the spectra based on the superposition of the contributions due to different Fe modifications (α- and a-Fe) will be discussed.

7.1. Temperature dependence of MOKE loops

Fig. 7.1 shows the polar Kerr ellipticity curves of the Tb-on-Fe (a) and Fe-on-Tb (b) bilayers obtained at $\lambda = 700$ nm and at T = RT (1) and 50 K (2). At a glance the polar ε_K curves of both samples present not only a common property, reversible magnetization reversal without hysteresis (in-plane magnetization) at both RT and T = 50 K, but also a difference. The ε_K amplitudes vary differently as a function of T. Whereas the saturation Kerr ellipticity, ε_K^s, of the Tb-on-Fe bilayer increases by more than 100% from 0.12° at RT to 0.25° at 50 K, ε_K^s of the Fe-on-Tb bilayer decreases from 0.17° at RT to 0.07° at T = 50 K, although the Fe layers in both samples show the same crystalline structure (bcc-Fe) as evidenced by CEMS measurements [Tapp98]. As will be discussed in Sec. 7.2 this is a mere spectroscopic effect, which is, again, due to the fact that the Fe layers are not homogeneous and that their components, α- and a-Fe, exhibit different spectral response curves (see Chapters 5 and 6).
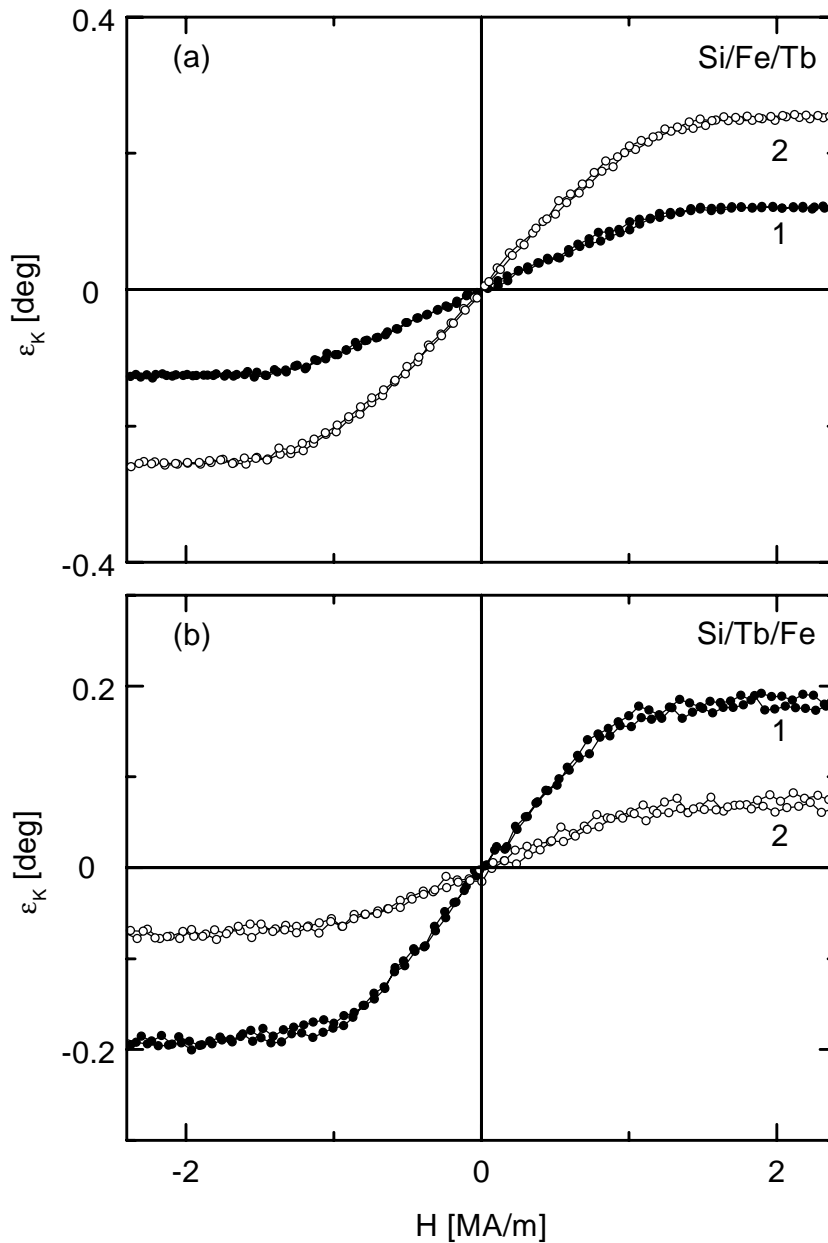
Fig. 7.1: *Polar Kerr ellipticity, ε_K, curves of Tb-on-Fe (a) and Fe-on-Tb bilayers (b) obtained at $\lambda = 700$ nm and $T = RT$ (1) and 50 K (2)*

When covering the Fe-on-Tb bilayer with one additional Tb-layer with $t_{Tb} = 1.4$ nm, Si/Tb/Fe/Tb, the shape of the Kerr curve at RT as shown in Fig. 7.2a, curve 1, indicates in-plane magnetization with a value of $H_s \approx 1$ MA/m being similar to that of the Fe-on-Tb bilayer (Fig. 7.1b, curve 1). However, at low temperature, $T = 50$ K (Fig. 7.2b, curve 1), the ε_K curve shows a hysteresis loop with a low coercive field, $H_c \approx 0.26$ MA/m. Obviously a reorientation transition from in-plane anisotropy at RT to PMA takes place upon lowering T. This is also

evidenced by CEMS measurement showing that the average canting angle of the α-Fe moments, $\langle\theta_{Fe}\rangle$, gradually changes from 90° at RT to $(43 \pm 3)°$ at T = 50 K (see Fig. 7.3) [Tapp98].

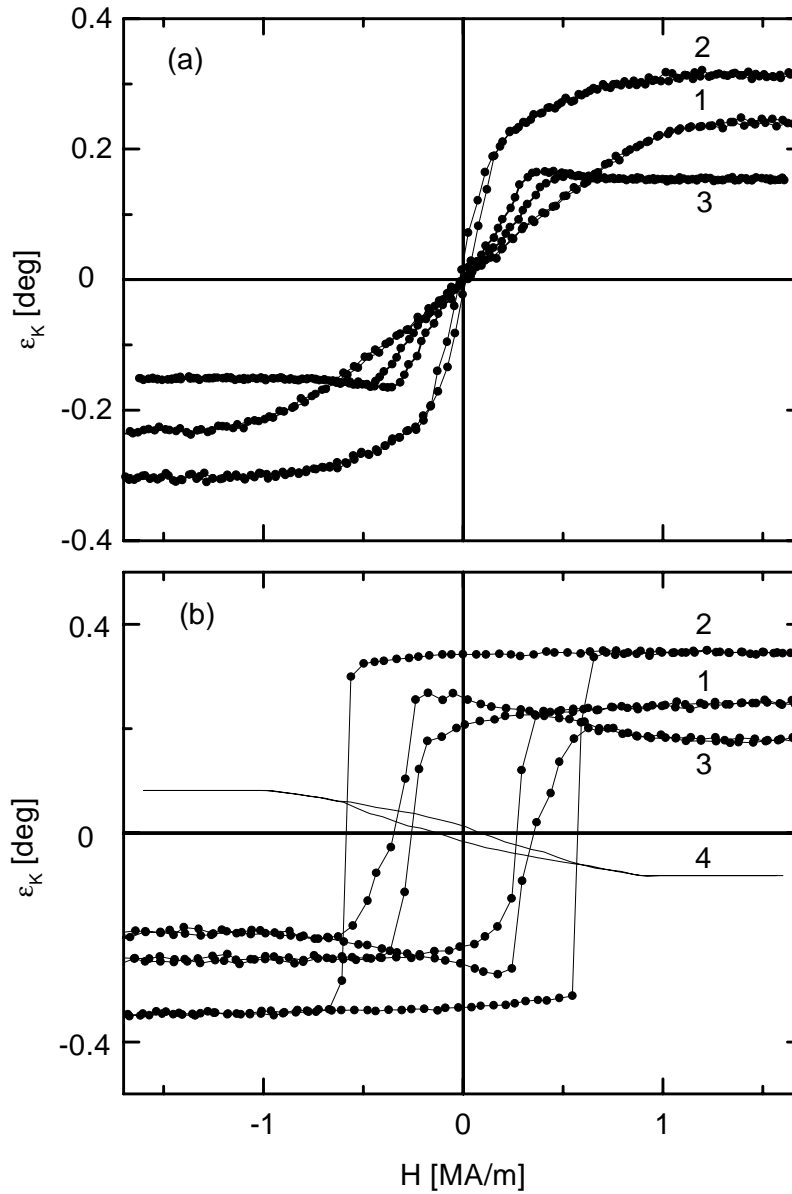*Fig. 7.2: Polar Kerr ellipticity, ε_K, curves of Si/[Tb/Fe]$_1$ + Tb (curves 1), Si/[Tb/Fe]$_3$ + Tb (curves 2) and Si/[Tb/Fe]$_{10}$ ($\equiv$ Ag3 in Chap. 6.2, curves 3)) obtained at T = RT (a) and 50 K (b) and at λ = 700 (curves 1 and 2) and 850 nm (3), respectively. Curve 4 (b) is calculated from curve 3 by subtracting a rectangular hysteresis loop like curve 2 properly weighted (see Chap. 6.2).*

At further increasing the number of Fe/Tb bilayers, n = 3, the ε_K curve reveals PMA even at RT (Fig. 7.2a, curve 2). At low temperature, T = 50 K, the ε_K curve shows a nearly perfectly rectangular hysteresis loop, $\varepsilon_K^s = \varepsilon_K^r$, with $H_c \approx 0.56$ MA/m, which is more than doubled when compared with that for n = 1. It is the largest H_c value shown in Fig. 7.2b (curve 2). In the case of the sample with n = 10 the value of H_c is reduced again by about 36% and amounts to about 0.36 MA/m at T = 50 K (Fig. 7.2b, curve 3). It should be noticed that the n = 10 sample is identical with the one denoted as „Ag3" previously (Chap. 6.2). Here we recall that a sizeable negative contribution to the total Kerr signal, ε_K^s, is due to the unavoidable a-Fe component (Fig. 7.2b, curve 4).

Remarkably, none of the MOKE loops measured at RT retains sizeable remanence, $\varepsilon_K^r \approx 0$, although hysteresis clearly hints at the influence of PMA for n = 3 and 10 (Fig. 7.2a, curves 2 and 3). Obviously, multidomain states are achieved under zero external field in order to minimize the dipolar magnetostatic energy [Hond90]. The observed shearing of the hysteresis loops, which is also typical of Co/Pt MLs with large n [Ochi89], can possibly be explained by magnetization reversals of single or multiple layers within the MLs stack [Grea92].

It should be remarked that in parallel to the non-monotonic behavior of H_c as a function of n also the Kerr ellipticity amplitude, ε_K^s, first rises and then decreases as n varies between 1 and 10. E. g. we find $\varepsilon_K^s = 0.24°$ for n = 1, $\varepsilon_K^s = 0.31°$ for n = 3, and $\varepsilon_K^s = 0.15°$ for n = 10 at RT (Fig. 7.2a). The reasons for this behavior are found in the complexity of both the magnetic structure and the magneto-optic response of the ML. The first increase of ε_K^s with n can roughly be explained by a simple addition of the MOKE contributions of the bilayers as reported in Co/Au MLs [Péni95]. The subsequent decrease of ε_K^s at further increasing n is probably caused by superposition of the MOKE signals of different ML components (see Chap. 6.2). Gradual changes of the single layer properties upon increasing the number of periods, n, were also observed in the framework of in-situ electrical resistivity measurements [Dufo91]. According to our spectroscopical studies (Chap. 7.2) the amounts of a-Fe intercalated between the grains of α-Fe increases as n increases, but seems to remain constant at n > 3.

The influence of n on the PMA was also investigated by CEMS measurements [Tapp98]. It was found that the perpendicular Fe-spin texture and the PMA first increase with the number of Fe/Tb interfaces, 2n -1. This is shown in Fig. 7.3 where $\langle\theta_{Fe}\rangle$ minimizes for n = 3.5 at RT and n = 2.5 at 50 K, then saturates at increasing n. This is also reflected by H_c obtained from Kerr ellipticity loops (Fig. 7.3, curve 3), because coercivity is closely associated with the anisotropy properties of magnetic materials. [Kron89, Mans95].
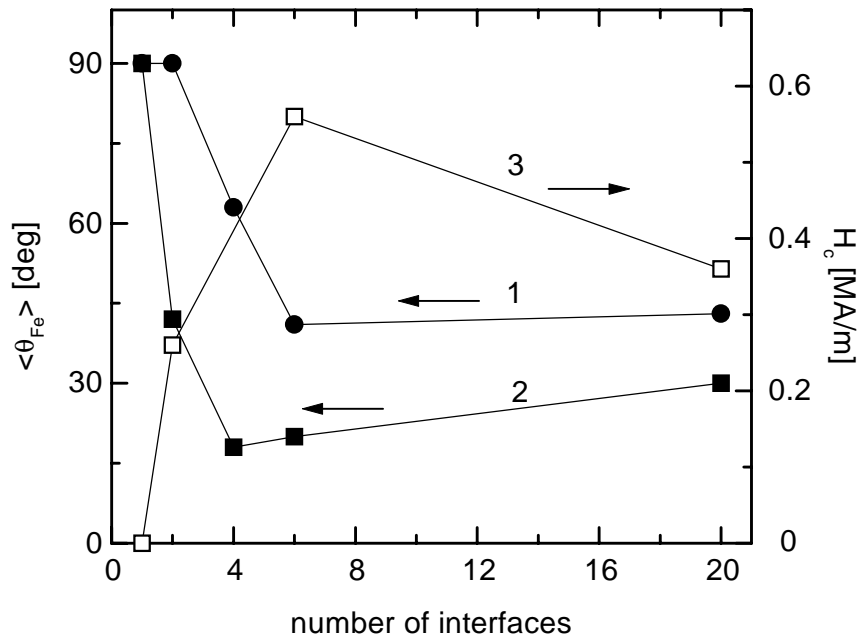

Fig. 7.3: Average canting angle $\langle\theta_{Fe}\rangle$ of the Fe-spin texture obtained by Mössbauer measurements at RT (curve 1) and 50 K (2) [Tapp98] and coercive fields H_c obtained from MOKE loops (Fig. 7.2b) at 50 K (curve 3) on samples with variant numbers of interfaces. The lines serve as guides to the eye.

Decreasing of PMA with increasing layer thickness is also observed in amorphous FeTb alloy films, where the angular dispersion of the local anisotropy takes place near the top surface when the film thickness is large, whereas the shape of hysteresis loops are alike for both top and bottom surfaces, when the film thickness is small [Take91].

It should be mentioned that the characteristic changes of the Kerr signal and of the PMA in dependence on the number of bilayers is not limited to Fe/Tb MLs but also occur in other magnetic MLs independent of their preparation conditions. Similar characteristic changes of both PMA and MOKE amplitude were also observed on Co/Pt and Co/Pd MLs by Ochiai et

al. [Ochi89] and on Co/Pt MLs by Greaves et al. [Grea93]. In these systems the optimum number n ≈ 10 for the PMA [Grun94] is somewhat larger than that of Fe/Tb MLs, where n = 3 seems to be optimum for PMA as determined by CEMS and MOKE measurements.

7.2. Wavelength dependence of MOKE signals

In Fig. 7.4 saturated polar Kerr ellipticity spectra $\varepsilon_K^s(\lambda)$ are shown. The curves 1-4 referring to samples with n < 10 reveal at first glance similar spectral behavior between $275 \leq \lambda \leq 600$ nm. In particular, a concave curvature with minimum at about $\lambda = 350$ nm is observed at both temperatures, RT (a) and T = 50 K (b). This spectral feature is similar to that of the bulk α-Fe (Fig. 7.4a, curve 6) [Krin65] and becomes increasingly obvious at increasing n up to n = 3. Contrastingly all of the curves systematically deviate from that of the bulk α-Fe in the long-wavelength range, $\lambda > 600$ nm. The spectra of the samples with only one interface, Tb-on-Fe (curves 1) and Fe-on-Tb (curves 2), and two interfaces, Tb/Fe/Tb ($\equiv$ n = 1, curves 3), show an increasing tendency with increasing wavelength. At further increasing the number of interfaces, n = 3 (curves 4), the Kerr spectra reveal a plateau at $\lambda > 650$ nm. Subsequently, the Kerr spectra for n = 10 (curves 5) drop down in this wavelength range. Simultaneously the amplitude of ε_K^s at short-wavelength is considerably shifted to higher values. Accordingly, their shape strongly deviates from that of the bulk α-Fe spectrum.

The spectral features of samples with n = 10 are independent of the thickness of their individual layers. E. g., the spectra of thick α-Fe/Tb MLs, [Fe(5.0)/Tb(2.6 nm)]$_{10}$ ($\equiv$ Y3, see Chap. 6.1), reveal nearly the same spectral behavior (not shown). For this reason interference effects are ruled out to be reason for the strong change of the spectral features between n = 3 and 10. We rather propose that they might roughly be understood as being due to the superposition of two different spectral contributions of variant Fe-modifications, α- and a-Fe, [Kim98b]. Whereas ε_K^s of α-Fe shows the typical S-shaped behavior discussed above (Fig. 7.4, curve 6), the ε_K^s spectra of a-Fe as encountered in the multilayer, [Fe(1.5)/Tb(1.9 nm)]$_{20}$ (Fig.6.11b, curve 2) show a monotonically decreasing tendency with λ as shown in Chap. 6.2 at both temperatures, RT and T = 50 K.
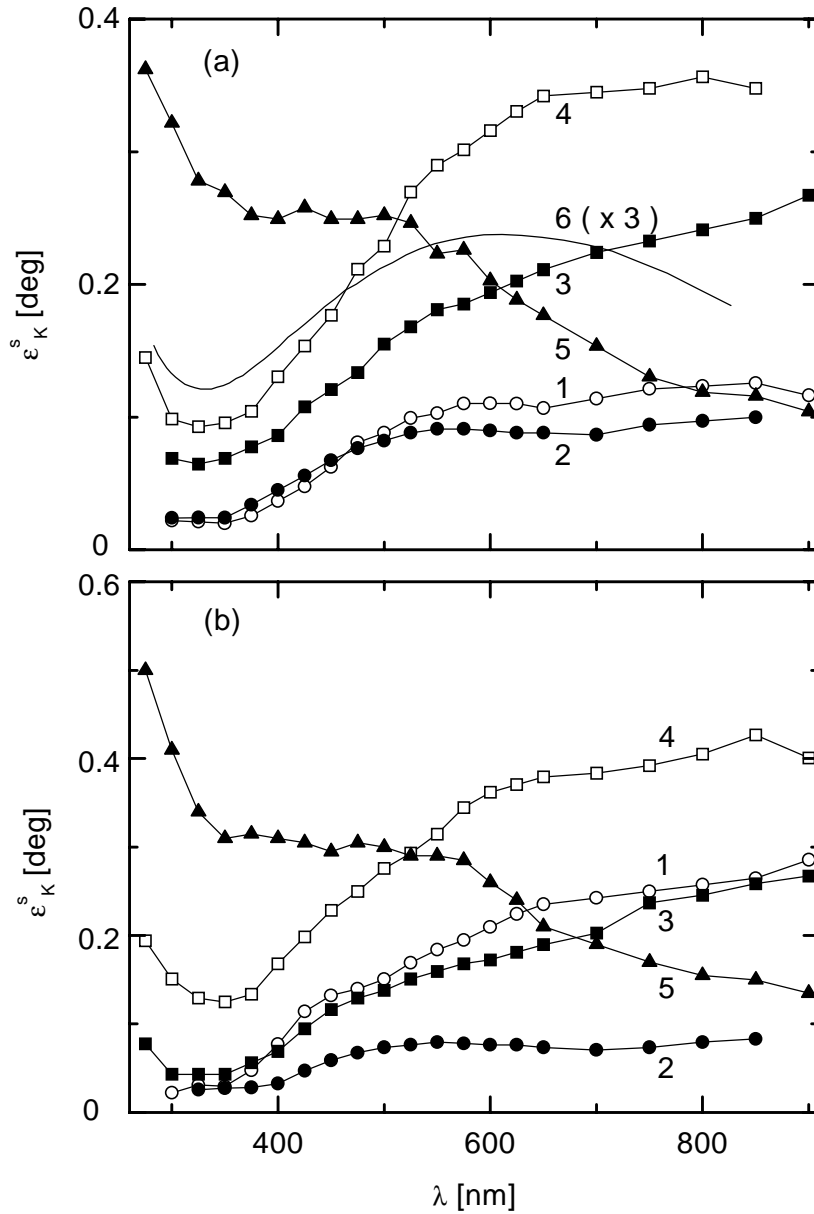
Fig. 7.4: Saturated polar Kerr ellipticity spectra, ε_K^s, of Tb-on-Fe (curve 1), Fe-on-Tb (2), Tb/Fe/Tb (3), [Tb/Fe]$_3$ + Tb (4) and [Tb/Fe]$_{10}$ (5) obtained at RT (a) and T = 50 K (b). The solid line (curve 6) shows the data of bulk α-Fe after Krinchik and Artem'ev [Krin65].

The possible origin of increasing contributions of a-Fe with n is probably due to the change in morphology of the Fe layers. Three experimental observations concerning to the structure of the Fe layers support this consideration:

(i) In situ resistance measurements on Tb/Fe/Tb triple layers show that the structure of the Fe layer near substrate is different from that of subsequent Fe layer [Dufo91].

(ii) CEMS measurements reveal that the average canting angle of the Fe spin-texture slightly increases with n after reaching a minimum at n = 2 (at RT) or 3(at 50 K) [Tapp98]. This hints at an increase of disorder of the Fe spin-texture. This is reflected in observation of canting angles close to the magic angle $<\theta_{Fe}> = 54.7°$ on thick a-Fe/Tb MLs [Scho91, Rich95], which indicates quasi-statistic orientational disorder of the Fe spin-texture although the Kerr loops show rectangular shapes (see Fig. 5.1).

(iii) The interfaces between Fe and Tb layers are expected to become increasingly rough in the uppermost layers for large n. This can lead to an increase of the canting angle of the Fe spin-texture (see above).

The consideration was already confirmed by x-ray diffraction on Co/Pt MLs [Hond90]. At this point it should be stressed that MOKE is particularly sensitive to the uppermost layers of a multilayer with non-negligible total thickness because of the finite penetration depth of light which is roughly 25 nm in the visible wavelength range [Trae92]. Hence, MOKE will reveal information on the most disordered parts of the MLs in the limit of large n, whereas magnetization measurements average over the whole volume.

Let us finally discuss the above question why the spectral properties of the bilayers Tb-on-Fe and Fe-on-Tb behave quite differently as a function of temperature. As shown by the hysteresis cycles in Fig. 7.1 and by the ε_K^s spectra in Fig. 7.4, the longer wavelength ($\lambda > 500$ nm) response decreases considerable when cooling the Fe-on-Tb from RT to 50 K, whereas ε_K^s slightly increases for the Tb-on-Fe sample. On the other hand, virtually no changes are observed on cooling of both of these samples when measuring ε_K^s in the near ultraviolet, $\lambda < 400$ nm.

Clearly, again, features due to the heterogeneity of the Fe components of these bilayers are encountered in these experiments. Roughly speaking, the near UV response reflects the MOKE of α-Fe which virtually does not change on cooling to below RT. However, in the near IR regime MOKE is primarily sensitive to the a-Fe components contained. Obviously, the rough interface characterizing the Fe-on-Tb bilayer favors a component, whose ε_K^s signal decreases with decreasing T. With respect to our previous discussions on the Fe/Tb ML system (Chap. 5, Fig. 5.4b) we are inclined to assume the existence of a virtually uncoupled a-

Fe component as encountered in the ML [Fe(3.0 nm)/Tb(1.9 nm)]$_{19}$. As shown in Fig. 5.4b its Kerr ellipticity, indeed, show the desired property. On the other hand, the observed increase of ε_K^s in the Tb-on-Fe bilayer containing a smooth interface seems to hint at a layer-like a-Fe component like that observed in the ML [Fe(1.5 nm)/Tb(1.9 nm)]$_{19}$ (Fig. 5.4a). This view seems to be corroborated by the observation that the near IR response of the trilayer Tb-Fe-Tb is nearly independent of temperature (Fig. 7.4, curves 3). Obviously the $\Delta\varepsilon_K^s$ effects of both kinds of interfaces with either sign just cancel.

Although the above inferences seem to follow quite plausibly from our previous discussions, the sizes of the effects are surprisingly large. It has to be stressed, however, that the Kerr spectroscopical probe strongly enhances the effects of the a-Fe components. As discussed in Chap. 5, these components are much less relevant in the magnetization curves, but they are clearly seen in Mössbauer spectroscopy. This method, however, does not distinguish between the two different species of a-Fe, which are quite obvious from the MOKE data. All of our experience seem to evidence two different morphologies, coherent layer-like a-Fe at smooth and incoherent precipitate-like a-Fe at rough interfaces.

It is interesting to interprete previous ε_K vs. H data obtained on a trilayer Si/Ag(20 nm)/Fe(3.5 nm)/Tb(1.4 nm) (Fig. 7.5) [Kim96] in the light of our above model. Whereas the change of slope, dε_K/dH, in the low-field range, $|H| < 0.8$ MA/m, from positive to negative when cooling the sample from 300 to 50 K, curves 1-3, was explained in terms of well-known (see also Sec. 5.2.2.) compensation phenomena, the decrease of ε_K^s at $|H| > 1.8$ MA/m with decreasing T remained unexplained. Here we suggest that, again, an amorphous Fe component with decreasing ε_K as T decreases is involved. Very probably it is formed as a precipitate-like component at the rough Ag/Fe interface, which seems to be compatible with Mössbauer investigations of Schurer et al. [Schu93, Schu95b]. It should be noticed that the T dependence of ε_K^s of the triple layer Ag/Fe/Tb (Fig. 7.5) resembles that of the bilayer Tb/Fe (Fig. 7.1b). On the other hand, the intercalation of Ag between the Si substrate and the Fe/Tb bilayer obviously enhances the PMA originating from the Fe/Tb interface. As discussed previously, the flat behavior of ε_K^s vs. H in the low-field range is due to wall movements of perpendicularly magnetized domains [Kim96]. Probably an effective reduction of t$_{Fe}$ due to

roughening of the interface at the Ag buffer [Schu93, Schu95b] enhances the weight of the surface anisotropy at the expense of the shape anisotropy energy.
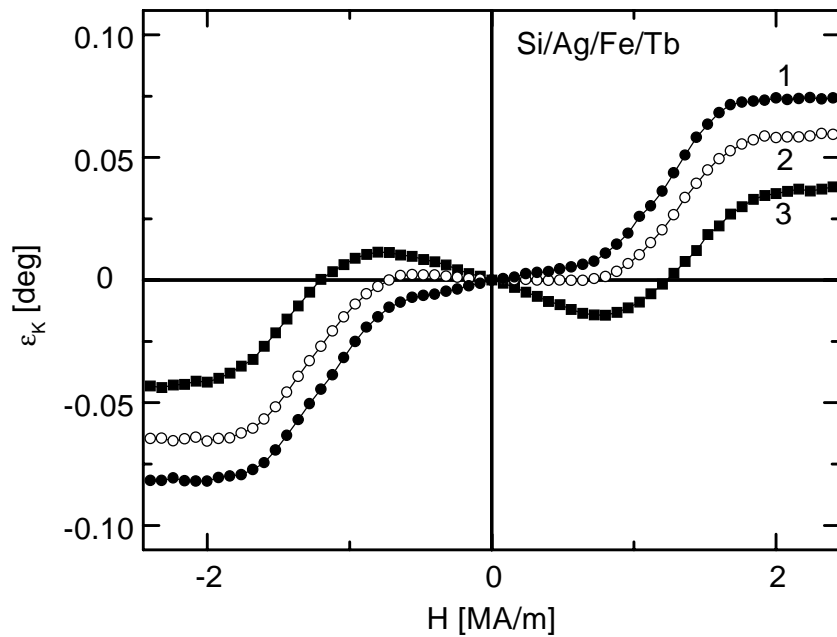

Fig. 7.5: Polar Kerr ellipticity ε_K of the Si/Ag (20 nm)/Fe(3.5 nm)/Tb(1.4 nm) obtained at a wavelength of 700 nm and at T = 300 (curve 1), 200 (2) and 50 K (3).